Through-The-Wall Radar Imaging With Wall Clutter Removal Via Riemannian Optimization On The Fixed-Rank Manifold

Hugo Brehier, Arnaud Breloy, Chengfang Ren, Guillaume Ginolhac

THROUGH-THE-WALL RADAR IMAGING WITH WALL CLUTTER REMOVAL VIA RIEMANNIAN OPTIMIZATION ON THE FIXED-RANK MANIFOLD

Hugo Brehier[1] *, Arnaud Breloy*[2]*, Chengfang Ren*[1]*, Guillaume Ginolhac*[3]

[1]SONDRA, CentraleSupélec, Univ. Paris-Saclay
[2]LEME, Univ. Paris-Nanterre
[3]LISTIC, Univ. Savoie Mont-Blanc

ABSTRACT

We introduce a new method for Through-the-Wall Radar Imaging (TWRI) that detects the location of stationary targets hidden by a wall. A crucial step is the mitigation of wall returns which obscure the scene and which are characterized by their low-rankedness given the radar measurement setup. Whereas existing methods make use of nuclear norm minimization or Truncated Singular Value Decomposition (TSVD), we propose to leverage Riemannian optimization over the manifold of fixed-rank matrices in order to use robust estimation while keeping the original rank constraint without relaxation. A detection step via sparse recovery is then performed and the overall method is compared with existing methods over simulated scenes. The results show that the proposed method achieves a better performance.

***Index Terms*—** Through-the-Wall Radar Imaging, Low rank approximation, Riemannian optimization, Robust estimation

1. INTRODUCTION

Through-the-Wall Radar Imaging (TWRI) [1] is a field of study whose main objective is to image a enclosed scene from its outside by using electromagnetic (EM) radiations in the radio-frequencies. The latter have the ability to partially penetrate common building materials while obtaining some reflections from the scene behind. There are difficulties arising from the interaction with the wall which imply some treatments in order to extract information about the scene enclosed.

Indeed, wall returns are overwhelming and have to be mitigated so as to image the scene behind. Moreover, the wall structure (e.g. rails on drywall) may create heterogeneous noise returns [2]. In this paper, we study the detection of stationary targets in a way that is robust to heterogeneous wall clutter. This topic of robustness has been studied for Ground Penetrating Radar [3,4] and TWRI [5] which added onto non-robust methods [6, 7]. In a setting of measures obtained parallel to the wall, front wall interferences form a low rank matrix. To migitate them, we propose to work on the Riemannian manifold of fixed-rank matrices. Our study on simulated data show the detection performance is enhanced by this method.

In the rest of this paper, Section 2 presents the signal model and existing work. Section 3 introduces the method proposed in this paper while Section 4 contains results and comparisons of this method with existing works.

2. SIGNAL MODEL AND EXISTING WORK

2.1. Signal model

We first describe a generic model for 2D TWRI [7,8]. A radar makes several measures sequentially over an axis parallel to the wall to penetrate with targets supposed to be few and small w.r.t. the scene dimensions as well as stationary. The returned signal for the m^{th} frequency and n^{th} position is written:

$$\begin{aligned} y(m,n) = &\sum_{k=1}^{K} \sigma_w^{(k)} \exp\left(-j\omega_m \tau_w^{(k)}\right) \\ &+ \sum_{i=1}^{R}\sum_{p=1}^{P} \sigma_p^{(i)} \exp(-j\omega_m \tau_{p,n}^{(i)}) \end{aligned} \tag{1}$$

with P the number of targets, K the number of reverberations in the wall and R the number of multipaths (e.g. via reflection on a side wall, see [9]). Additionally, $\sigma_w^{(k)}$ and $\tau_w^{(k)}$ are the complex overall attenuation coefficient and round-trip delay for the wall returns associated with the k^{th} reverberation while $\sigma_p^{(i)}$ and $\tau_{p,n}^{(i)}$ are those associated with the p^{th} target, i^{th} multipath and n^{th} radar position.

We discretize those returns over a grid of dimension (N_x, N_z) covering the scene via a dictionary $\mathbf{\Psi}$. For the i^{th} multipath scheme and the n^{th} transceiver position, its $(n_x, n_z)^{th}$ column describes the return from a point target at the $(n_x, n_z)^{th}$ pixel which can be solved approximately via geometrical optic considerations [6]. The overall model is then written compactly as [5, Eq. 5]:

$$\mathbf{Y} = \mathbf{L} + \mathbf{\Psi}\left(\mathbf{I}_N \otimes \mathbf{r}\right) \tag{2}$$

where $\mathbf{Y} \in \mathbb{C}^{M\times N}$ is the data matrix, $\mathbf{L} \in \mathbb{C}^{M\times N}$ is the matrix of front wall returns which is low-rank, as wall returns

are invariant along the displacement axis, and $\mathbf{r} \in \mathbb{C}^{N_x N_z R}$ the vector containing the scene returns amplitude (associated to the dictionary $\mathbf{\Psi}$) which is sparse as few targets are present.

2.2. Previous work

A previously proposed method for robust and one-step wall mitigation and target detection for TWRI in [5] is through a robust data fitting in a decoupled convex relaxation:

$$\begin{aligned} \min_{\mathbf{L},\mathbf{R},\mathbf{M},\mathbf{S}} \quad & \|\mathbf{M}\|_* + \lambda \|\mathbf{S}\|_{2,1} \\ & + \frac{\mu}{2} \sum_{i,j} H_c([\mathbf{Y} - \mathbf{L} - \mathbf{\Psi}(\mathbf{I}_N \otimes \mathrm{vec}(\mathbf{R}))]_{ij}) \\ \text{s.t.} \quad & \mathbf{M} = \mathbf{L}, \quad \mathbf{S} = \mathbf{R} \end{aligned} \tag{3}$$

where $\|\cdot\|_*$ is the nuclear norm (the sum of singular values), known to be the convex envelope of the rank [10]. Furthermore, $\|\cdot\|_{2,1}$ is the $\ell_{2,1}$ mixed-norm (the sum of Euclidean norm of the rows) as the ℓ_1-norm is the convex envelope of the ℓ_0 'norm'. It induces row-wise sparsity, which is across multipaths in our case, as they represent the same underlying physical scene and should activate together [7]. Moreover, H_c is the so-called Huber function [11] with threshold c:

$$H_c(x) = \begin{cases} \frac{1}{2}|x|^2 & \text{if } |x| \leq c \\ c(|x| - \frac{1}{2}c) & \text{if } |x| > c \end{cases} \tag{4}$$

We can use the Alternating Directions Method of Multipliers (ADMM) framework [12] to solve it (see [5] for the details). This has the advantage of having closed-form updates for $\mathbf{L}, \mathbf{M}, \mathbf{S}$ via proximal operators [13]. For $\mathbf{R}$, we can tailor a Majorization-Minimization [14] scheme which removes the need for a gradient descent and a step-size to tune.

However, this may slightly degrade performance due to the convex relaxation and the decoupling of variables. We can bypass the need for those elements by considering directly the non-convex optimisation of the rank constraint.

3. NEW ROBUST TWRI METHOD VIA RIEMANNIAN OPTIMIZATION

The overall, not convexly relaxed, optimization problem is:

$$\begin{aligned} & \min_{\mathbf{L},\mathbf{R}} \sum_{ij} H_c([\mathbf{Y} - \mathbf{L} - \mathbf{\Psi}(\mathbf{I} \otimes \mathrm{vec}(\mathbf{R}))]_{ij}) \\ & \text{s.t. } \mathrm{rk}(\mathbf{L}) = k \ , \ \|\mathbf{R}\|_{2,0} \leq l \end{aligned} \tag{5}$$

which can be tackled via a Block Coordinate Descent (BCD) over $\mathbf{L}$ and $\mathbf{R}$. We first study the optimization over $\mathbf{L}$ in a non-convex manner.

3.1. Wall mitigation : riemannian estimation of L

3.1.1. Problem statement

The problem we are interested in, over $\mathbf{L}$, is then:

$$\min_{\mathbf{L} \in \mathbb{C}_k^{M \times N}} f(\mathbf{L}) = \sum_{i,j} H_c([\mathbf{Y} - \mathbf{\Psi}(\mathbf{I}_N \otimes \mathrm{vec}(\mathbf{R})) - \mathbf{L}]_{ij}) \tag{6}$$

where $\mathbb{C}_k^{M \times N} = \{\mathbf{X} \in \mathbb{C}^{M \times N} : \mathrm{rk}\,(\mathbf{X}) = k\}$. Notice that we went from a non-fixed low rank optimization to a fixed-rank constraint. A way to directly tackle the fixed-rank constraint is via Riemannian optimization [15]. Such geometrical consideration allows for elegant algorithmic solutions, as the space $\mathbb{C}_k^{M \times N}$ forms a Riemannian manifold. Moreover, we have a good a priori of the true rank of the low-rank matrix $\mathbf{L}$ from the knowledge of the physical setup. This will not require a convex relaxation of the rank nor a decoupling variable.

3.1.2. Algorithmic resolution

Via the truncated SVD of rank $k \leq n$, we can parameterize a fixed-rank matrix as:

$$\mathbf{L} \overset{\text{TSVD}}{=} \mathbf{U}(\mathbf{\Sigma}\mathbf{W})^H = \mathbf{U}\mathbf{V}^H \tag{7}$$

The most commonly used and practical algorithm for Riemannian optimization is Riemannian Gradient Descent (RGD) whose j^{th} iteration is:

$$(\mathbf{U}, \mathbf{V})_{j+1} = \mathrm{R}_{(\mathbf{U},\mathbf{V})_j}(-\alpha_j P^h_{(\mathbf{U},\mathbf{V})_j}(P^t_{(\mathbf{U},\mathbf{V})_j}(\nabla f((\mathbf{U}, \mathbf{V})_j)))) \tag{8}$$

with ∇f denoting the *Euclidean* gradient of f and α_k a step size found by line-search. $P^t_{(\mathbf{U},\mathbf{V})_j}(\cdot)$ is the projection from ambient space to tangent space while $P^h_{(\mathbf{U},\mathbf{V})}(\cdot)$ is the projection from the tangent space to the horizontal space and $\mathrm{R}_{(\mathbf{U},\mathbf{V})}(\cdot)$ denotes the retraction of a horizontal vector to the manifold (notions we expand on in the next section) at the point $(\mathbf{U}, \mathbf{V})$.

Note that the method has local convergence [15] and that we used a refined initialization to the rank-k truncated SVD of the data matrix. We thus need to compute the Euclidean gradient of f from which will follow the Riemannian gradient.

Proposition 1. *The Euclidean gradient is found via Wirtinger calculus [16] as* $\nabla f = (\frac{\partial f}{\partial \mathbf{U}^*}, \frac{\partial f}{\partial \mathbf{V}^*})$ *with:*

$$\frac{\partial f}{\partial \mathbf{U}^*} = \sum_{ij} H_c'([\mathbf{U}\mathbf{V}^H - \tilde{\mathbf{Y}}]_{ij})([\mathbf{J}^{mn}\mathbf{V}^T]_{ij})_{mn} \tag{9}$$

$$\frac{\partial f}{\partial \mathbf{V}^*} = \sum_{ij} H_c'([\mathbf{U}\mathbf{V}^H - \tilde{\mathbf{Y}}]^*_{ij})([\mathbf{J}^{mn}\mathbf{U}^T]_{ji})_{mn} \tag{10}$$

where $\tilde{\mathbf{Y}} = \mathbf{Y} - \mathbf{\Psi}(\mathbf{I} \otimes \mathbf{r})$ *and* $\mathbf{J}^{mn}$ *is the single-entry matrix which has* 1 *at the* $(m,n)^{th}$ *entry and* 0 *elsewhere. Moreover* $[\mathbf{A}]_{ij}$ *extracts the* $(i,j)^{th}$ *entry of* $\mathbf{A}$ *whereas* $(\mathbf{A})_{mn}$ *constructs a matrix entry by entry.*

Proof. Let the problem be:

$$\min_{\mathbf{U},\mathbf{V}} \; f(\mathbf{U},\mathbf{V}) = \sum_{ij} H_c([\mathbf{U}\mathbf{V}^H - \tilde{\mathbf{Y}}]_{ij}) \tag{11}$$

Denote $z = [\mathbf{U}\mathbf{V}^H - \tilde{\mathbf{Y}}]_{ij}$. Then via Wirtinger calculus and its chain rule, we find the steepest ascent direction:

$$\frac{\partial f}{\partial \mathbf{U}^*} = \sum_{ij} \left(\frac{\partial H_c(z,z^*)}{\partial z}\frac{\partial z}{\partial \mathbf{U}^*} + \frac{\partial H_c(z,z^*)}{\partial z^*}\frac{\partial z^*}{\partial \mathbf{U}^*} \right) \tag{12}$$

$\frac{\partial H_c(z,z^*)}{\partial z^*}$ is equivalent to $H_c'(z)$, the derivative of the real Huber function, while $\frac{\partial H_c(z,z^*)}{\partial z}$ is equivalent to $H_c'(z^*)$.

Note that $\frac{\partial z}{\partial \mathbf{U}^*} = \frac{\partial [\mathbf{U}\mathbf{V}^H - \tilde{\mathbf{Y}}]_{ij}}{\partial \mathbf{U}^*} = \mathbf{0}$. Moreover $\frac{\partial z^*}{\partial [\mathbf{U}^*]_{mn}} = \frac{\partial [\mathbf{U}^*\mathbf{V}^T - \tilde{\mathbf{Y}}]_{ij}}{\partial [\mathbf{U}^*]_{mn}} = [\mathbf{J}^{mn}\mathbf{V}^T]_{ij}$ We can then construct the whole matrix $\frac{\partial z^*}{\partial \mathbf{U}^*}$ elementwise. Thus:

$$\frac{\partial f}{\partial \mathbf{U}^*} = \sum_{ij} H_c'([\mathbf{U}\mathbf{V}^H - \tilde{\mathbf{Y}}]_{ij})([\mathbf{J}^{mn}\mathbf{V}^T]_{ij})_{mn} \tag{13}$$

And similarly:

$$\frac{\partial f}{\partial \mathbf{V}^*} = \sum_{ij} H_c'([\mathbf{U}\mathbf{V}^H - \tilde{\mathbf{Y}}]^*_{ij})([\mathbf{J}^{mn}\mathbf{U}^T]_{ji})_{mn} \tag{14}$$

□

3.1.3. Manifold parametrization

Note that (7) leads to the subspace projection parameterization of the fixed-rank matrix manifold, described in [17, 18] whereas another possibility is the embedded one [15, 19].

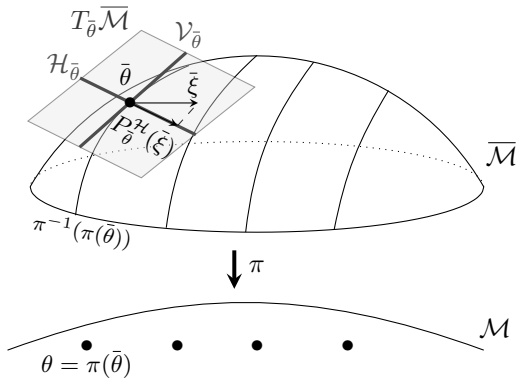

Fig. 1. A generic quotient manifold $\mathcal{M}$ embedded in its total space $\overline{\mathcal{M}}$ and the decomposition of the tangent space at a point $\bar\theta$ in the direction $\bar\xi$

.

We briefly review it. Since (7) is invariant under an orthogonal factor, it gives rise to the quotient space (cf. Figure 1):

$$\mathrm{St}(m,k) \times \mathbb{C}^{n\times k}_* / \mathcal{O}(k) \tag{15}$$

with the Stiefel manifold $\mathrm{St}(m,k) = \{\mathbf{X} \in \mathbb{C}^{m\times k} : \mathbf{X}^H\mathbf{X} = \mathbf{I}_k\}$, the manifold of full rank matrices $\mathbb{C}^{n\times k}_* = \{\mathbf{C} \in \mathbb{C}^{n\times k} : \mathrm{rk}(\mathbf{C}) = k\}$ and the orthogonal group $\mathcal{O}(k) = \{\mathbf{X} \in \mathbb{C}^{k\times k} : \mathbf{X}^H\mathbf{X} = \mathbf{I}_k\}$. Its tangent space can be decomposed into:

$$\mathrm{T}_{(\mathbf{U},\mathbf{V})}(\mathrm{St}(m,k) \times \mathbb{C}^{n\times k}_*) = \mathrm{T}_{\mathbf{U}}\,\mathrm{St}(m,k) \times \mathbb{C}^{n\times k} \tag{16}$$

with the tangent space of the Stiefel manifold $\mathrm{T}_{\mathbf{U}}\,\mathrm{St}(m,k) = \{\mathbf{U}\boldsymbol{\Omega} + \mathbf{U}_\perp\mathbf{W} : \boldsymbol{\Omega} \in \mathcal{A}(k), \mathbf{W} \in \mathbb{C}^{(m-k)\times k}\}$ and the tangent space of the manifold of full rank matrices $\mathrm{T}_{\mathbf{U}}\,\mathbb{C}^{n\times k}_* = \mathbb{C}^{n\times k}$ where $\mathcal{A}(k) = \{\mathbf{X} \in \mathbb{C}^{k\times k} : \mathbf{X}^H = -\mathbf{X}\}$ is the set of skew-symmetric matrices of size $k \times k$ which is the orthogonal complement of $\mathcal{O}(k)$.

Projection onto the tangent space is then:

$$P^t_{(\mathbf{U},\mathbf{V})}(\dot{\mathbf{U}},\dot{\mathbf{V}}) = (\dot{\mathbf{U}} - \mathbf{U}\,\mathrm{sym}(\mathbf{U}^H\dot{\mathbf{U}}), \dot{\mathbf{V}}) \tag{17}$$

where $\mathrm{sym}(\mathbf{A}) = \frac{1}{2}(\mathbf{A}^H + \mathbf{A})$.

A fiber of this quotient manifold is $\{(\mathbf{U}\mathbf{O}, \mathbf{V}\mathbf{O}) : \mathbf{O} \in \mathcal{O}(k)\}$ and the vertical space $\mathcal{V}_{(\mathbf{U},\mathbf{V})}$ is the space tangent to the fiber: $\mathcal{V}_{(\mathbf{U},\mathbf{V})} = \{(\mathbf{U}\boldsymbol{\Omega}, \mathbf{V}\boldsymbol{\Omega}) : \boldsymbol{\Omega} \in \mathcal{A}(k)\}$. This parametrization may be endowed with the metric:

$$\bar{g}_{(\mathbf{U},\mathbf{V})}((\dot{\mathbf{U}},\dot{\mathbf{V}}),(\tilde{\mathbf{U}},\tilde{\mathbf{V}})) = \mathrm{tr}(\dot{\mathbf{U}}^H\tilde{\mathbf{U}}) + \mathrm{tr}((\mathbf{V}^H\mathbf{V})^{-1}\dot{\mathbf{V}}^H\tilde{\mathbf{V}}) \tag{18}$$

where the first term is the standard euclidean metric and the second term the natural metric on full rank matrices which renders it invariant to a change of basis. The horizontal space $\mathcal{H}_{(\mathbf{U},\mathbf{V})}$ which we want to work in, is then the orthogonal complement to $\mathcal{V}_{(\mathbf{U},\mathbf{V})}$ w.r.t. the metric, which gives:

$$\begin{aligned}\mathcal{H}_{(\mathbf{U},\mathbf{V})} = \{&(\dot{\mathbf{U}},\dot{\mathbf{V}}) \in \mathbb{C}^{m\times k} \times \mathbb{C}^{n\times k} : \\ &\mathbf{U}^H\dot{\mathbf{U}} \in \mathcal{A}(k), \mathbf{U}^H\dot{\mathbf{U}} + \mathbf{V}^H\dot{\mathbf{V}} \in \mathcal{O}(k)\}\end{aligned} \tag{19}$$

Note that we can write the projection onto the horizontal space and along the vertical space, for some $\boldsymbol{\Omega} \in \mathcal{A}(k)$ as :

$$P^h_{(\mathbf{U},\mathbf{V})}(\dot{\mathbf{U}},\dot{\mathbf{V}}) = (\dot{\mathbf{U}} - \mathbf{U}\boldsymbol{\Omega}, \dot{\mathbf{V}} - \mathbf{V}\boldsymbol{\Omega}) \tag{20}$$

Using the property that $P^h_{(\mathbf{U},\mathbf{V})}(\dot{\mathbf{U}},\dot{\mathbf{V}}) \in \mathcal{H}_{(\mathbf{U},\mathbf{V})}$ it follows after some rearrangement that we may obtain $\boldsymbol{\Omega}$ by solving a nested symmetric Lyapunov equation:

$$\begin{aligned}(\mathbf{V}^H\mathbf{V})\tilde{\boldsymbol{\Omega}} + \tilde{\boldsymbol{\Omega}}(\mathbf{V}^H\mathbf{V}) = &\,2\,\mathrm{skew}((\mathbf{V}^H\mathbf{V})(\dot{\mathbf{U}}^H\mathbf{U})(\mathbf{V}^H\mathbf{V})) \\ &- 2\,\mathrm{skew}((\dot{\mathbf{V}}^H\mathbf{V})(\mathbf{V}^H\mathbf{V}))\end{aligned} \tag{21a}$$

$$\tilde{\boldsymbol{\Omega}} = (\mathbf{V}^H\mathbf{V})\boldsymbol{\Omega} + \boldsymbol{\Omega}(\mathbf{V}^H\mathbf{V}) \tag{21b}$$

where $\mathrm{skew}(\mathbf{A}) = \frac{1}{2}(\mathbf{A}^H - \mathbf{A})$. Finally, we introduce a retraction of horizontal vectors onto the manifold. In our case, it can be decomposed in terms of the retractions of the components $\mathrm{St}(m,k)$ and $\mathbb{C}^{n\times k}_*$ which can be found in [20, section 4.1.2]. For $(\bar{\mathbf{U}},\bar{\mathbf{V}}) \in \mathcal{H}_{(\mathbf{U},\mathbf{V})}$, it is:

$$\mathrm{R}_{(\mathbf{U},\mathbf{V})}(\bar{\mathbf{U}},\bar{\mathbf{V}}) = (\mathrm{uf}(\mathbf{U} + \bar{\mathbf{U}}), \mathbf{V} + \bar{\mathbf{V}}) \tag{22}$$

where uf extracts the unitary factor (of the polar decomposition) of a full column rank matrix.

3.2. Target detection : Sparse r-step via PGD

The target detection is achieved in a standard row-wise sparse reconstruction step. No sparse Riemannian manifold exist, we therefore cannot use such methods for this step. We may use a row-wise hard-thresholding [21, Definition 2] but it showed to underperform while other non-convex methods [22] use a least squares data fitting. We thus resort to the classical convex relaxation over the $\ell_{2,1}$-norm, as described in Section 2.2. It is then possible to use proximal gradient descent (PGD) for the minimization over this variable. We will denote this method as HBCD for Huber-BCD.

The minimization problem over $\mathbf{R}$ in regularized form is:

$$\min_{\mathbf{R}} \quad \sum_{p_i \in \mathcal{P}} H_c(\|[\mathbf{Y} - \mathbf{L} - \mathbf{\Psi}(\mathbf{I}_N \otimes \mathrm{vec}(\mathbf{R}))]_{p_i}\|_F) + \lambda \|\mathbf{R}\|_{2,1} \tag{23}$$

We consider the vectorized variable $\mathbf{r} = \mathrm{vec}(\mathbf{R})$ in order to compute the gradient which we then unvectorize in order to apply the proximal step. At iteration $t+1$, we have :

$$\mathbf{R}_{t+1} = T_{\lambda s}\left(\mathrm{vec}^{-1}\left(\mathbf{r}_t - s\mathbf{g}_t\right)\right) \tag{24}$$

where T is the proximal of the $\ell_{2,1}$-norm, s is a step-size that can be found by line-search (which does not vary over iterations in practice so that it can be fixed) and $\mathbf{g}$ is the needed gradient of the robust fitting term.

Proposition 2. *The steepest ascent direction* $\mathbf{g}$ *is:*

$$\mathbf{g} = -\sum_{p_i \in \mathcal{P}} \frac{H_c'(\|[\mathbf{E}]_{p_i}\|_F)}{\|[\mathbf{E}]_{p_i}\|_F} \left(\sum_{(j,k) \in p_i} [\mathbf{E}]_{j,k} (\mathbf{\Psi}_k)_{j,:}^H \right) \tag{25}$$

where $\mathbf{E} = \mathbf{Y} - \mathbf{L} - \mathbf{\Psi}(\mathbf{I}_N \otimes \mathbf{r})$ *and* $(\mathbf{\Psi}_k)_{j,:}$ *denotes the* j^{th} *line of* $\mathbf{\Psi}_k$.

Proof. The derivation can be found in [5]. □

4. SIMULATIONS

We test the method on Finite-Difference Time-Domain [23] (FDTD) simulated data obtained via GprMax [24] while the Riemannian optimization is carried out with Pymanopt [25] which we completed by transposing the real manifolds to the complex case.

We compare SRCS [6] as well as KRPCA [7] and HKRPCA (as seen in Section 2.2) to the method of this paper, HBCD, with rank fixed to either 1 or 2 (as denoted by the suffixes rk1 or rk2). We generate heterogeneous noise following a student-t distribution with 2.1 degrees of freedom (d.f.) which is a renowned distribution having heavier tails [2] than the normal distribution (for finite d.f.). We consider a point-wise structure of the noise, whereas column-wise (by radar position) may be alternatively considered.

Sample detection maps are displayed in Figure 2 which show promising results: it appears that the method HBCD proposed in this paper better handles the heterogeneous noise (which follows here a student-t distribution with 2.1 degrees of freedom (d.f.) which is a renowned distribution having heavier tails than the normal distribution for finite d.f.). We

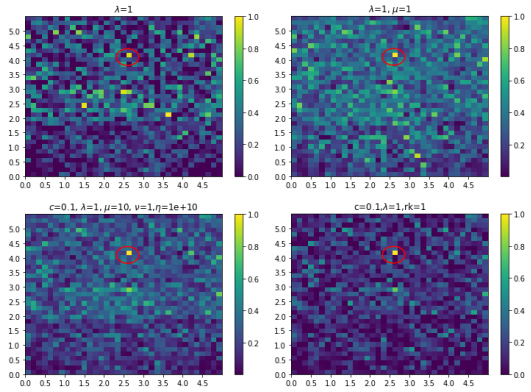

Fig. 2. Detection maps with student-t noise with 2.1 d.f. and SNR of 10 dB (top-left: SRCS, top-right: KRPCA, bottom-left: HKRPCA, bottom-right: HBCD)

perform a quantitative study by constructing the Receiver Operator Characteristic (ROC) of the different methods. Each point on the curve is the results of a Monte-Carlo average over 60 draws of noise. At a specific Signal to Noise Ratio (SNR) we observe the better performance of the method proposed here.

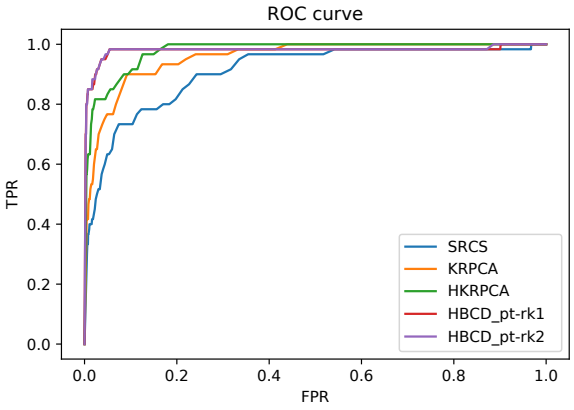

Fig. 3. ROC with student-t noise with 2.1 d.f. and 60 Monte-Carlo samples and SNR = 10 dB

5. CONCLUSION

We developed a new robust method for TWRI which leverages the performance of Riemannian optimization over fixed-rank matrices. Detection results achieved in a standard detection step show its advantage in a context of heterogeneous noise.

6. REFERENCES

[1] M.G. Amin, *Through-the-Wall Radar Imaging*, CRC Press, 2017.

[2] Esa Ollila, David E. Tyler, Visa Koivunen, and H. Vincent Poor, "Complex elliptically symmetric distributions: Survey, new results and applications," *IEEE Transactions on Signal Processing*, vol. 60, no. 11, pp. 5597–5625, 2012.

[3] Q. Hoarau, G. Ginolhac, A.M. Atto, and J.M. Nicolas, "Robust adaptive detection of buried pipes using GPR," *Signal Processing*, vol. 132, pp. 293–305, 2017.

[4] Matthieu Gallet, Ammar Mian, Guillaume Ginolhac, Esa Ollila, and Nickolas Stelzenmuller, "New robust sparse convolutional coding inversion algorithm for ground penetrating radar images," *IEEE Transactions on Geoscience and Remote Sensing*, vol. 61, pp. 1–14, 2023.

[5] Hugo Brehier, Arnaud Breloy, Chengfang Ren, and Guillaume Ginolhac, "Through the wall radar imaging via Kronecker-structured Huber-type RPCA," *Signal Processing*, p. 109228, 2023.

[6] Moeness G. Amin and Fauzia Ahmad, "Compressive sensing for through-the-wall radar imaging," *Journal of Electronic Imaging*, vol. 22, no. 3, pp. 1 – 22, 2013.

[7] Hugo Brehier, Arnaud Breloy, Chengfang Ren, Israel Hinostroza, and Guillaume Ginolhac, "Robust PCA for Through-the-Wall Radar Imaging," in *2022 30th European Signal Processing Conference (EUSIPCO)*, 2022, pp. 2246–2250.

[8] Van Ha Tang, Abdesselam Bouzerdoum, and Son Lam Phung, "Compressive radar imaging of stationary indoor targets with low-rank plus jointly sparse and total variation regularizations," *IEEE Transactions on Image Processing*, vol. 29, pp. 4598–4613, 2020.

[9] Michael Leigsnering, Fauzia Ahmad, Moeness Amin, and Abdelhak Zoubir, "Multipath exploitation in through-the-wall radar imaging using sparse reconstruction," *IEEE Transactions on Aerospace and Electronic Systems*, vol. 50, no. 2, pp. 920–939, 2014.

[10] Maryam Fazel, *Matrix rank minimization with applications*, Ph.D. thesis, PhD thesis, Stanford University, 2002.

[11] Ricardo A Maronna, R Douglas Martin, Victor J Yohai, and Matías Salibián-Barrera, *Robust statistics: theory and methods (with R)*, John Wiley & Sons, 2019.

[12] Stephen Boyd, Neal Parikh, Eric Chu, Borja Peleato, and Jonathan Eckstein, "Distributed optimization and statistical learning via the alternating direction method of multipliers," *Found. Trends Mach. Learn.*, vol. 3, no. 1, pp. 1–122, Jan. 2011.

[13] Neal Parikh and Stephen Boyd, "Proximal algorithms," *Found. Trends Optim.*, vol. 1, no. 3, pp. 127–239, Jan. 2014.

[14] Y. Sun, P. Babu, and D. Palomar, "Majorization-minimization algorithms in signal processing, communications, and machine learning," *IEEE Trans. on Signal Process.*, vol. PP, no. 99, pp. 1–1, 2016.

[15] Nicolas Boumal, *An introduction to optimization on smooth manifolds*, Cambridge University Press, 2023.

[16] Raphael Hunger, "An introduction to complex differentials and complex differentiability," Tech. Rep. TUM-LNS-TR-07-06, 2007.

[17] Bamdev Mishra, Gilles Meyer, Silvère Bonnabel, and Rodolphe Sepulchre, "Fixed-rank matrix factorizations and riemannian low-rank optimization," *Computational Statistics*, vol. 29, 09 2012.

[18] P. Absil, Luca Amodei, and Gilles Meyer, "Two newton methods on the manifold of fixed-rank matrices endowed with riemannian quotient geometries," *Computational Statistics*, vol. 29, 09 2012.

[19] Bart Vandereycken, "Low-rank matrix completion by riemannian optimization," *SIAM Journal on Optimization*, vol. 23, no. 2, pp. 1214–1236, 2013.

[20] P.-A. Absil, R. Mahony, and R. Sepulchre, *Optimization Algorithms on Matrix Manifolds*, Princeton University Press, Princeton, NJ, 2008.

[21] Wenwen Min, Taosheng Xu, Xiang Wan, and Tsung-Hui Chang, "Structured sparse non-negative matrix factorization with $\ell_{2,0}$-norm," *IEEE Transactions on Knowledge and Data Engineering*, vol. 35, no. 8, pp. 8584–8595, 2023.

[22] Xiaoqin Zhang, Jingjing Zheng, Di Wang, Guiying Tang, Zhengyuan Zhou, and Zhouchen Lin, "Structured sparsity optimization with non-convex surrogates of $\ell_{2,0}$-norm: A unified algorithmic framework," *IEEE Transactions on Pattern Analysis and Machine Intelligence*, vol. 45, no. 5, pp. 6386–6402, 2023.

[23] Kane Yee, "Numerical solution of initial boundary value problems involving maxwell's equations in isotropic media," *IEEE Transactions on Antennas and Propagation*, vol. 14, no. 3, pp. 302–307, 1966.

[24] Craig Warren, Antonios Giannopoulos, and Iraklis Giannakis, "gprMax: Open source software to simulate electromagnetic wave propagation for ground penetrating radar," *Computer Physics Communications*, vol. 209, pp. 163–170, 2016.

[25] James Townsend, Niklas Koep, and Sebastian Weichwald, "Pymanopt: A python toolbox for optimization on manifolds using automatic differentiation," *Journal of Machine Learning Research*, vol. 17, no. 137, pp. 1–5, 2016.